A Search for Neutron-Antineutron Oscillation in the NOvA Experiment

Dung Duc Phan
(On behalf of the NOvA Collaboration)

The University of Texas at Austin

ICISE Webinar
September 3rd, 2020

Motivation

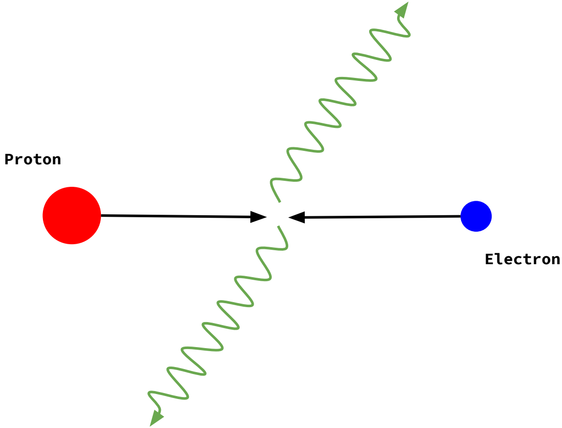

Motivation

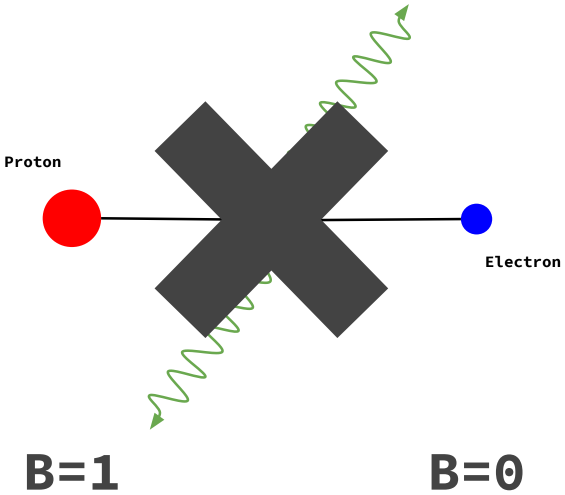

Motivation

Stability of matter originated the baryon number B and its conservation law.

- $B = (-)1/3$ for (anti)quarks,
  $B = 0$ for others.
- Total B must not change.

Why we question this conservation?

- Noether's theorem: B conservation lacks an associated symmetry.
- Sakharov's conditions: Observed matter-antimatter asymmetry requires B violation, CP violation, and thermal inequilibrium.

Emmy Noether

Andrei Sakharov

Why Neutron-Antineutron Oscillation?

Stringent experimental limits ruled out many models of proton decays.

Neutron-antineutron oscillation search.

- A viable probe to $\Delta B = 2$
- $\Delta(B - L) = 2$ with multiple new physics in a single ($0\nu2\beta$, ν mass mechanism, $n - \bar{n}$) framework
- Probing the TeV physics regime.

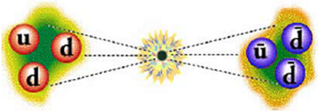

Neutron Oscillation Phenomenology

The Schroedinger equation for the $n, \bar{n}$ system can be written as

$$i \frac{\partial}{\partial t} \begin{pmatrix} n \\ \bar{n} \end{pmatrix} = \begin{pmatrix} E_n & \delta m \\ \delta m & E_{\bar{n}} \end{pmatrix} \begin{pmatrix} n \\ \bar{n} \end{pmatrix} = A \begin{pmatrix} n \\ \bar{n} \end{pmatrix} \tag{1}$$

The solution can be written as

$$\begin{pmatrix} n \\ \bar{n} \end{pmatrix}_t = \mathrm{e}^{-iAt} \begin{pmatrix} n \\ \bar{n} \end{pmatrix}_{t=0} \tag{2}$$

where e^{iAt} is a 2×2 matrix. If the system starts as n, i.e. $(1, 0)$, the probability of being detected as $\bar{n}$, i.e. $(0, 1)$, is

$$P_{\bar{n}}(t) = \left| \begin{pmatrix} 0 & 1 \end{pmatrix} \mathrm{e}^{-iAt} \begin{pmatrix} 1 \\ 0 \end{pmatrix} \right|^2 \tag{3}$$

Neutron Oscillation Phenomenology

For free neutrons

$$P_{\bar{n}}(t) \sim \left(\frac{t}{\tau_{n\bar{n}}}\right)^2 \tag{4}$$

where the free neutron oscillation life-time $\tau_{n\bar{n}} = 1/\delta m$.

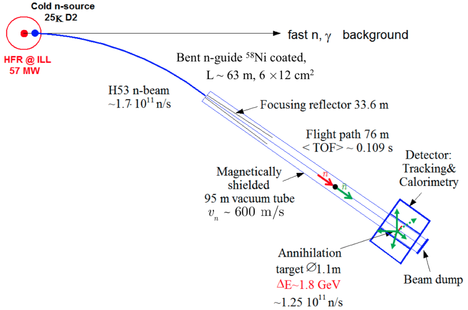

Figure 1: Setup of a free neutron oscillation experiment (ILL/Grenoble).

Neutron Oscillation Phenomenology

For bound neutrons, we can treat them as being free for very short

$$\delta t \sim \frac{1}{E_{\text{binding}}} \sim \frac{1}{10\ \text{MeV}} \sim 10^{-22}\,\text{s} \tag{5}$$

So a bound neutron experiences this free condition for $R \sim 1/\delta t \sim 10^{22}$ times per second. The oscillation probability per second is then:

$$P_{\bar{n}}(t) \equiv \frac{1}{T_{n\bar{n}}} = \left(\frac{\delta t}{\tau_{n\bar{n}}}\right)^2 \frac{1}{\delta t} = \frac{1}{\tau_{n\bar{n}}^2 \times R} \tag{6}$$

The oscillation life-time of bound neutrons $T_{n\bar{n}}$ relates to that of free neutrons $\tau_{n\bar{n}}$ via the nuclear suppression factor $R \sim 10^{22}\,\text{s}^{-1}$

$$T_{n\bar{n}} = \tau_{n\bar{n}}^2 \times R \tag{7}$$

Neutron Oscillation Search in NOvA

- On surface detector.
- No previous attempts.
- A different nucleus. A different detection technique.
- Promising competitive results.

Experiment	Source of neutrons	T (yr)	τ (s)
ILL	neutron beam		0.9×10^8
Soudan	^{56}Fe	0.72×10^{32}	1.3×10^8
Frejus	^{56}Fe	0.65×10^{32}	1.2×10^8
Kamiokande	^{16}O	0.43×10^{32}	1.2×10^8
Super-K	^{16}O	1.90×10^{32}	2.7×10^8
SNO	^{2}D	1.48×10^{31}	1.4×10^8
NOvA	^{12}C	?	?

Table 1: Experimental limits on neutron oscillation life-time.

NOvA Experiment

The NOvA Experiment

NuMI **O**ff-axis ν_e **A**ppearance

- Far Detector 14 kton
- Near Detector 300 ton
- Baseline 810 km
- Off-axis NuMI $\nu_\mu, \bar{\nu}_\mu$ beam

Detector Design

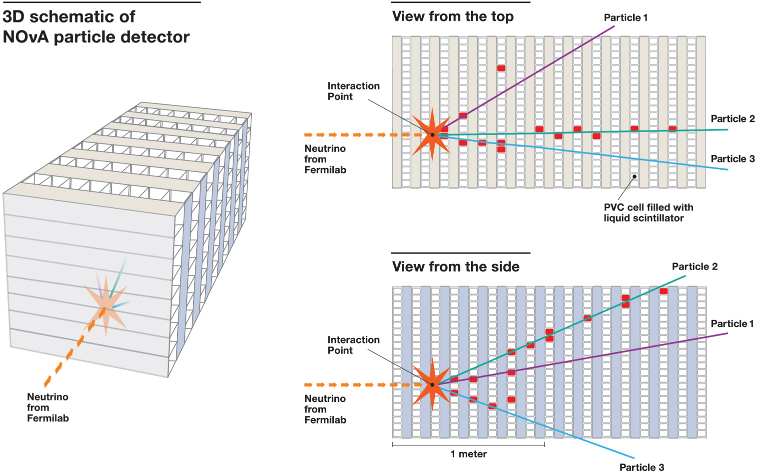

Detector Design

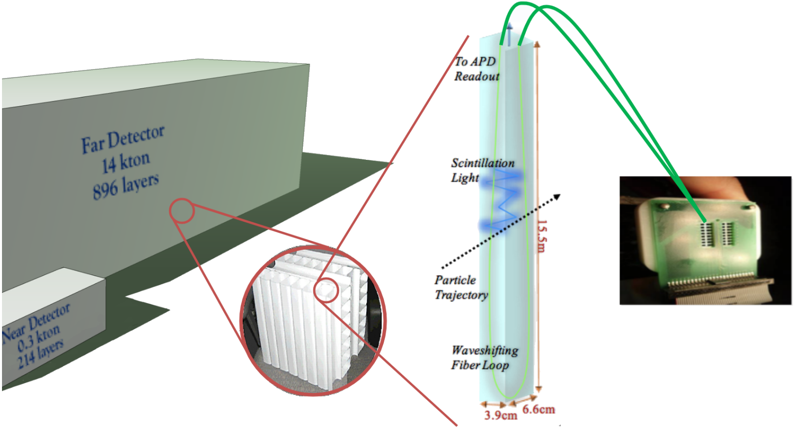

Visualization of Event in NOvA

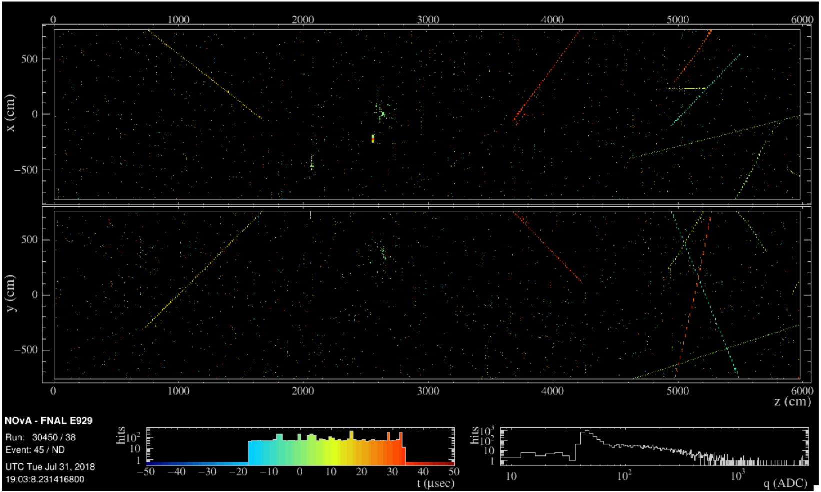

Figure 2: Display of a real data event record.

Physics at NOvA

ν_μ, $\bar{\nu}_\mu$ disappearance

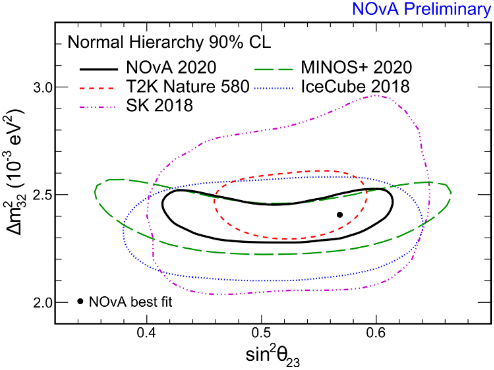

ν_e, $\bar{\nu}_e$ appearance

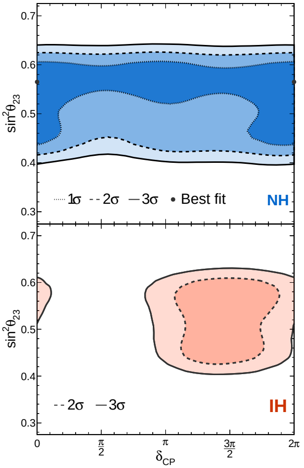

Exotics Physics Search

- Dark Matter, Magnetic Monopoles
- Multimessenger Astrophysics: Gravitational Wave and Supernova.
- Neutron-Antineutron Oscillation

NNbar Simulation

- Visualize a signal event in the detector.
- Understand its characteristics.

NNbar Simulation

$\bar{n}+p$		$\bar{n}+n$	
$\pi^+\pi^0$	1%	$\pi^+\pi^-$	2%
$\pi^+2\pi^0$	8%	$2\pi^0$	1.5%
$\pi^+3\pi^0$	10%	$\pi^+\pi^-\pi^0$	6.5%
$2\pi^+\pi^-\pi^0$	22%	$\pi^+\pi^-2\pi^0$	11%
$2\pi^+\pi^-2\pi^0$	36%	$\pi^+\pi^-3\pi^0$	28%
$2\pi^+\pi^-2\omega$	16%	$2\pi^+2\pi^-$	7%
$3\pi^+2\pi^-\pi^0$	7%	$2\pi^+2\pi^-\pi^0$	24%
		$\pi^+\pi^-\omega$	10%
		$2\pi^+2\pi^-2\pi^0$	10%

Table 2: The branching ratios for the $\bar{n}$+nucleon annihilations. Derived from measurements of $\bar{p}$+nucleon annihilations using isospin symmetry.

NNbar Simulation

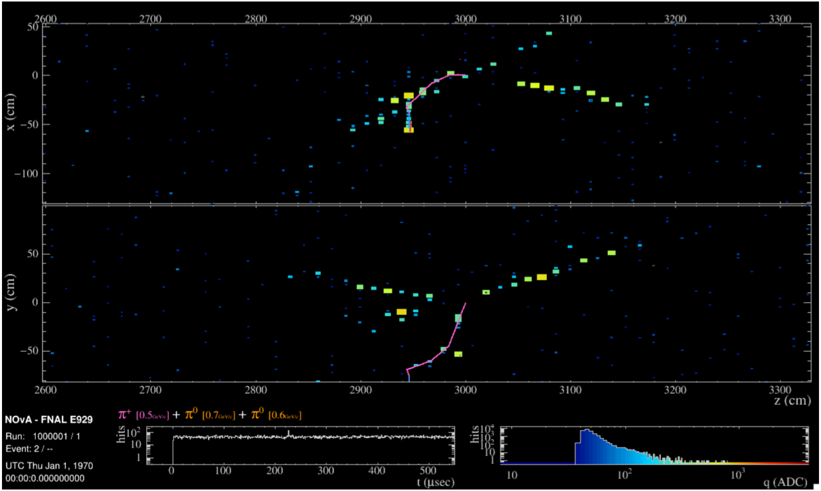

Figure 3: Display of a $p + \bar{n} \rightarrow \pi^{+} + 2\pi^{0}$ simulated event.

Characteristics of Signals in the Detector

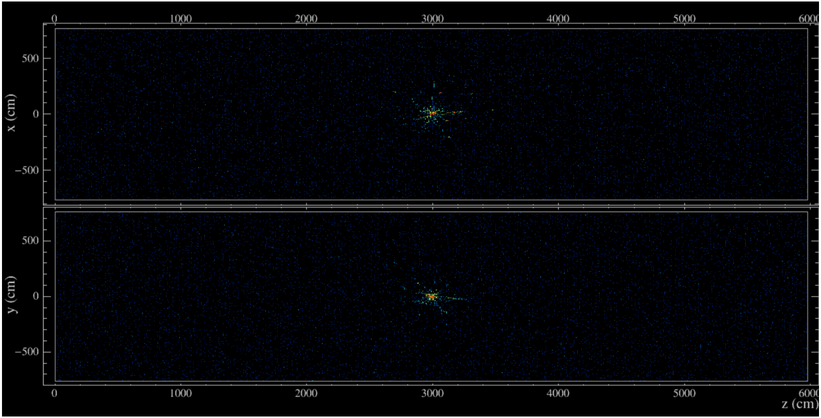

Figure 4: Overlay of 10 signal events at the same vertex.

Characteristics of Signals in the Detector

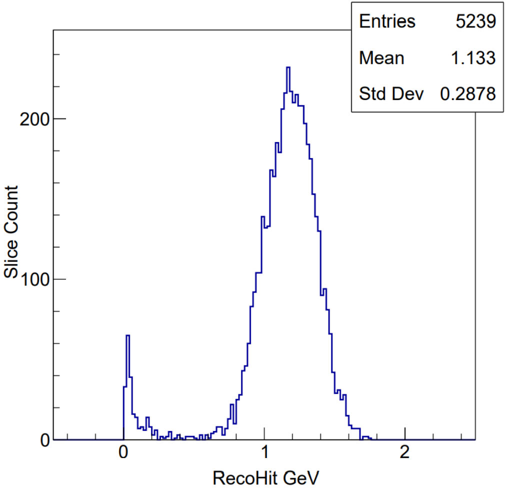

Figure 5: Visible Energy of Signal Events.

Trigger Development

Neutron Oscillation Trigger

The Neutron Oscillation Trigger or `NNbarDDT` has strict performance requirements

- Be able to reduce the high cosmic muon background rate of 120 kHz down to the assigned trigger rate of 5 Hz.
- Ensure a decent signal efficiency ($> 50\%$).

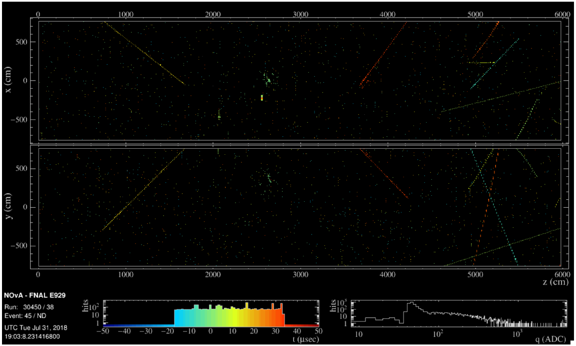

Figure 6: Display of a real data event record.

Trigger Selection Cuts

Containment Cut

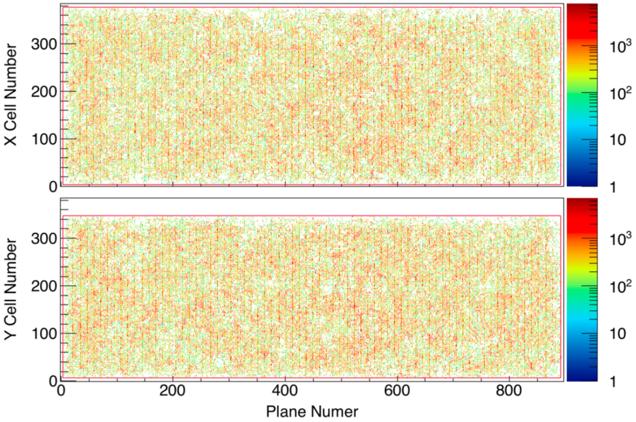

Figure 7: The red lines indicate the boundary of the containment volume. Rate reduction: 120 kHz → 3.2 kHz. Signal efficiency 68%.

Trigger Selection Cuts

2 - Width-to-Length Ratio Cut

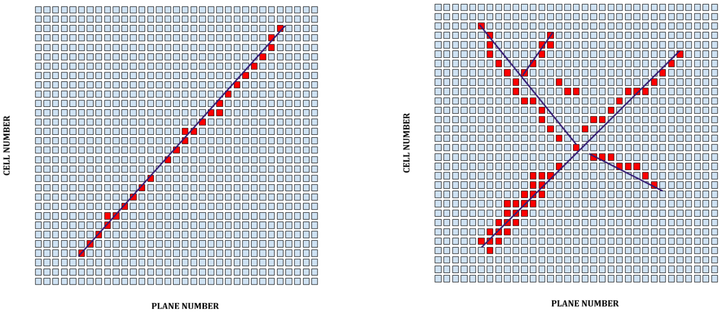

Figure 8: Cartoon display of cosmic (left) and signal (right) events in a certain detector view. Hough transform is applied to find the line features embedded. The length of the longest Hough line is defined as the length L. The largest distance from any hits to that Hough line is defined as the width W.

Trigger Selection Cuts

2 - Width-to-Length Ratio Cut

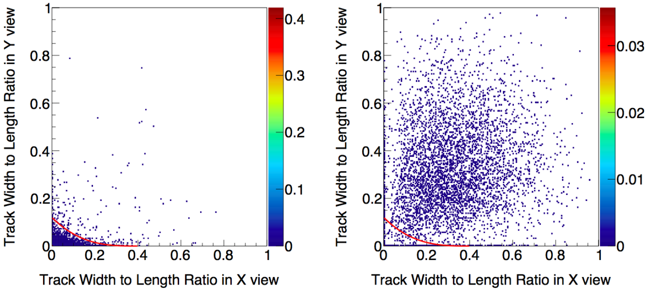

(a) cosmic (b) signal

Figure 8: Slices in the region below the red curve are cut off (99% cosmic rays and 10% signal).

Trigger Selection Cuts

Cell Number Multiplicity

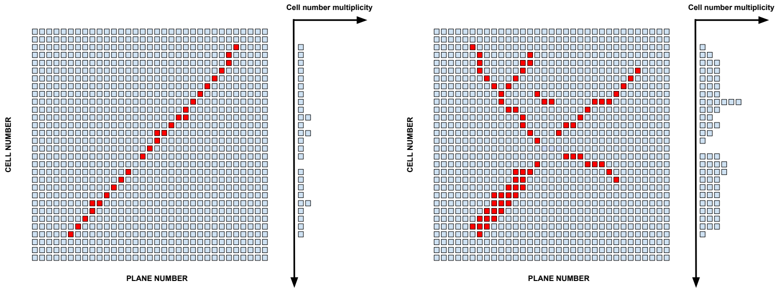

Figure 9: A cartoon of display of a background cosmic (left) and a signal (right) to demonstrate the concept of cell number multiplicity.

$$M = \frac{N_{\mathrm{multiple}}}{N_{\mathrm{total}}}, \tag{8}$$

Trigger Selection Cuts

Cell Number Multiplicity

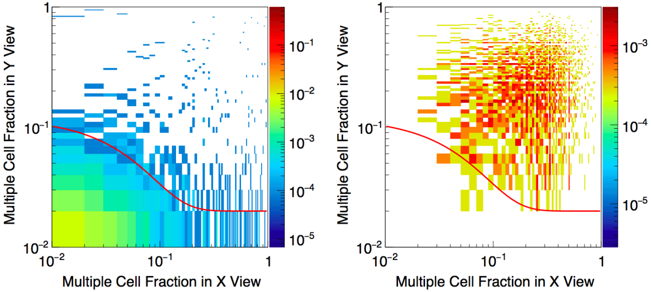

(a) cosmic (b) signal

Figure 9: Slices in the region below the red curve are cut off (97% of cosmic rays and 4% of signal candidates).

Trigger Selection Cuts

Hit Count Asymmetry

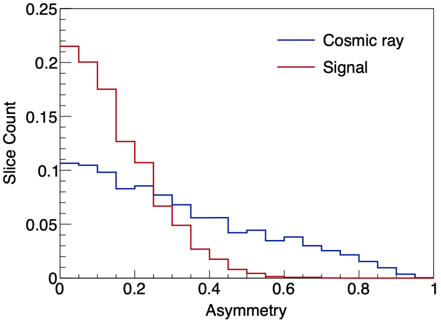

Figure 10: $a \to 0$ signifies a quite symmetrical event geometry. Slices with $a > 0.5$ are cut off (21% of cosmic rays and 0.6% of signal candidate).

Performance of the Neutron Oscillation Trigger

Selection cuts	Trigg. Rate (Hz)	Signal Eff. (%)
Pre-containment	118637	100
Containment	3167	68
Width-length ratio	21	61
Cell number multiplicity	9	59
Hit count asymmetry	7	59
Hit extent asymmetry	5	57

Table 3: Trigger Rate and Signal Efficiency after successive application of selection cuts.

Performance of the Neutron Oscillation Trigger

Triggered Events

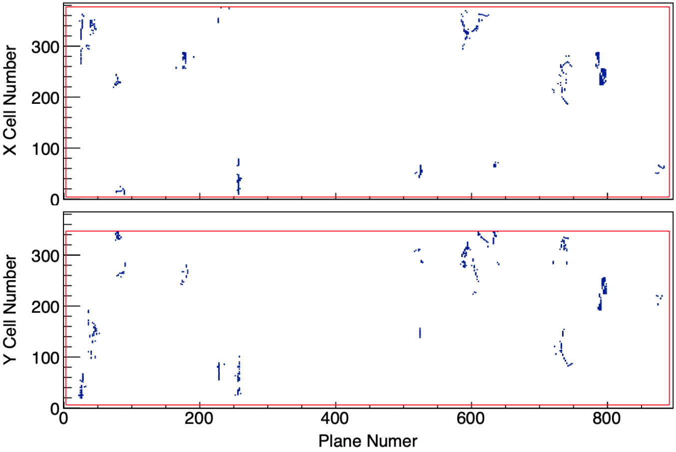

Figure 11: Hits of the remaining 15 cosmic slices after all the cuts. Red lines indicates the boundary of the containment volume.

Sensitivity Analysis

Analysis Approach

Due to the lack of a solid background modelling, real data is partially unblinded for the analysis development.

- Dataset from 4 months of FD exposure (15% of total data collected so far) is used for this study.
- It is unblinded under "all-background" assumption and serving the purpose of a data-driven background study.
- Signal dataset contains simulated events from all 16 $\bar{n}$ annihilation channels is used to evaluate the signal efficiency of the event selector.

Event Reconstruction

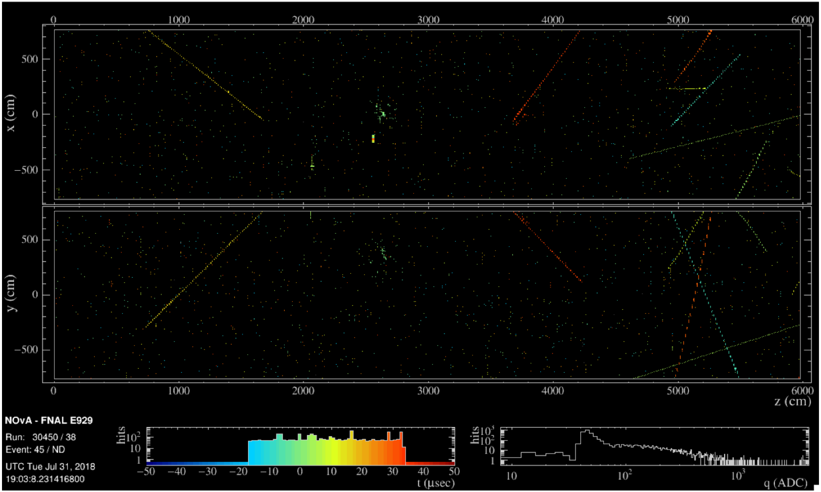

Event Reconstruction

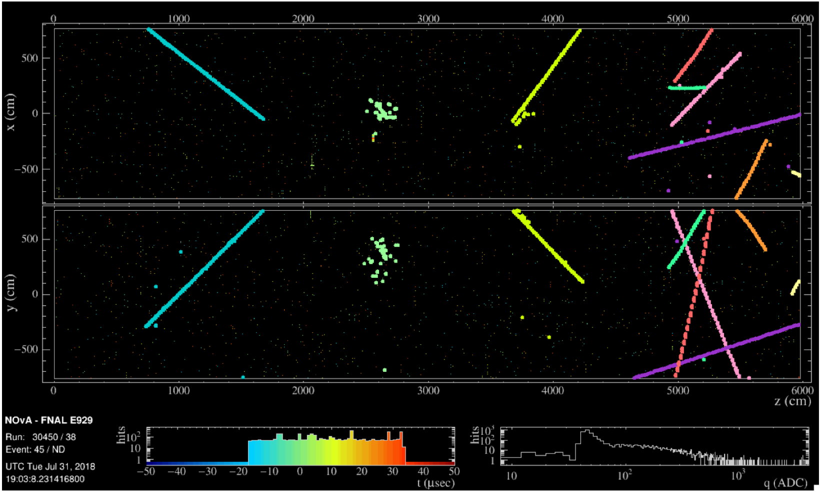

Event Reconstruction

Vertex Reconstruction

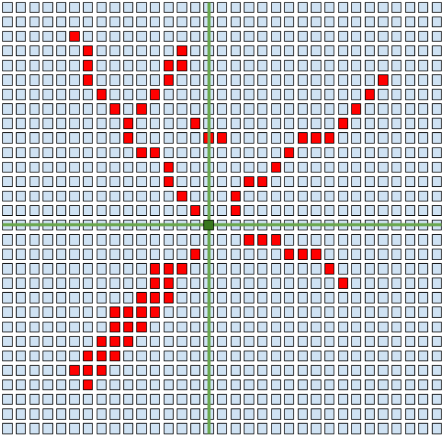

Figure 12: Vertex's position is the "energy balancing point".

Event Reconstruction

Vertex Reconstruction

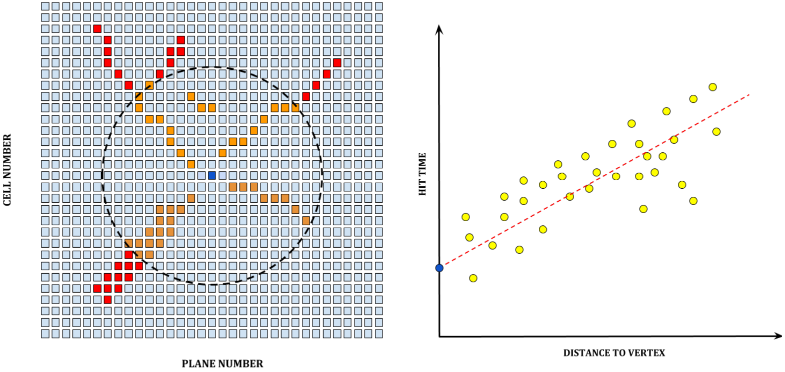

Figure 12: Vertex's timing. In the event display (left) the blue point is the vertex's position. The energy sum of hits within dashed circle is 50% of total energy. Selected hits are marked in orange. Timing regression (right) is performed to find the timing of the vertex.

Selection Variables

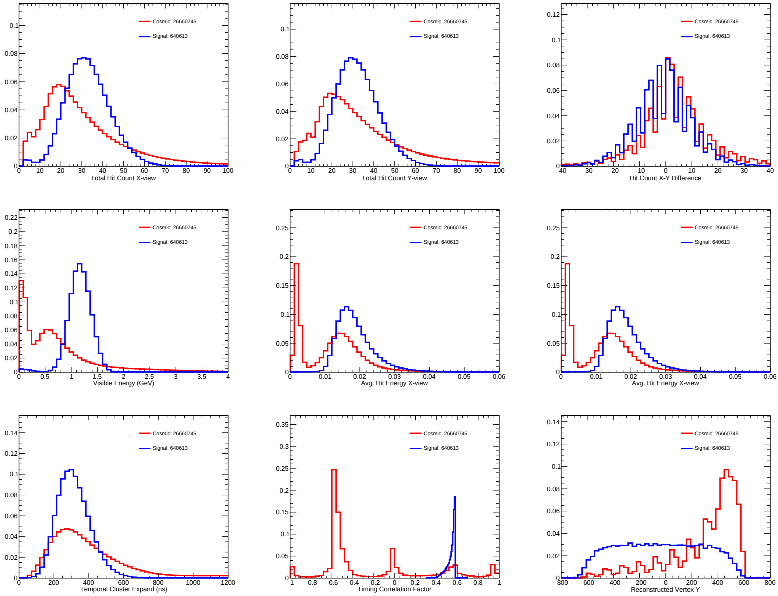

Selection Cuts

Cut 1	$\texttt{TotalHitCountInXView} < 55$
Cut 2	$\texttt{TotalHitCountInYView} < 55$
Cut 3	$\texttt{HitCountXYDifference} < 10$
Cut 4	$0.9\,\text{GeV} < \texttt{TotalVisibleEnergy} < 1.6\,\text{GeV}$
Cut 5	$14\,\text{MeV} < \texttt{AverageEnergyPerHitYView} < 40\,\text{MeV}$
Cut 6	$12\,\text{MeV} < \texttt{AverageEnergyPerHitXView} < 40\,\text{MeV}$
Cut 7	$\texttt{EventDuration} < 550\,\text{ns}$
Cut 8	$0.47 < \texttt{PositionTimingCorrelationFactor} < 0.58$
Cut 9	$-600\,\text{cm} < \texttt{ReconVertexY} < -150\,\text{cm}$

Table 4: The selection cut applied on each variable.

- Background: 63 candidate events found ($\sim$ 190 evts/yr).
- Signal Eff. of 20.2%. Overall = DDT $\times$ 20.2% = 11.5%.

Selection Variables - After Selection Cuts

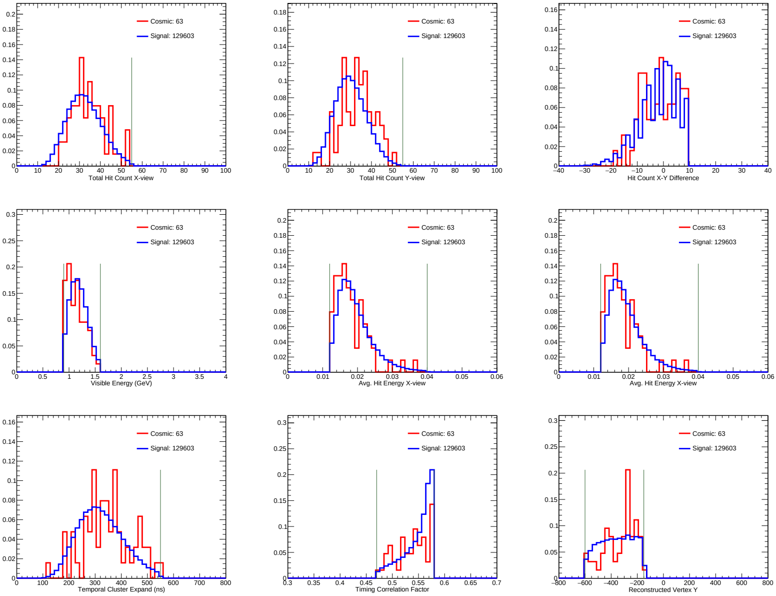

Some Selected Candidates

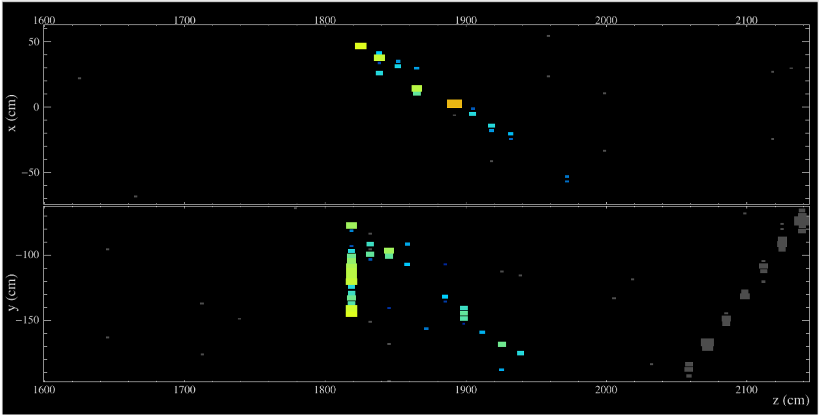

Some Selected Candidates

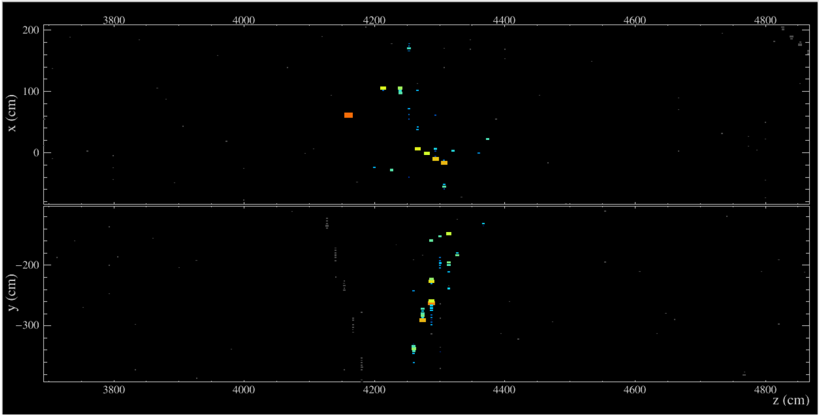

Some Selected Candidates

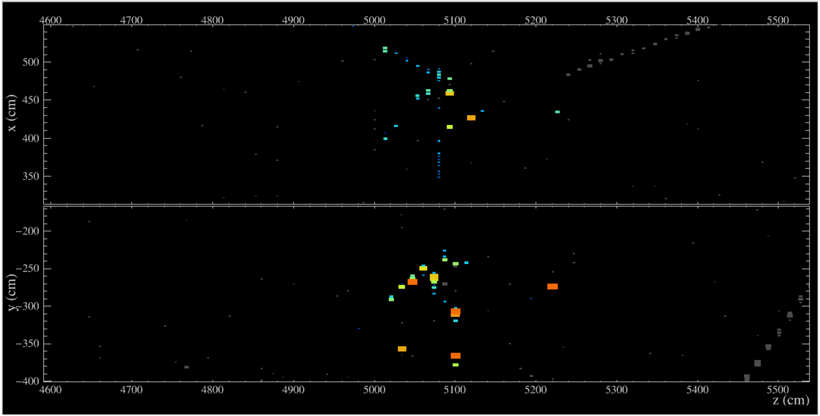

Some Selected Candidates

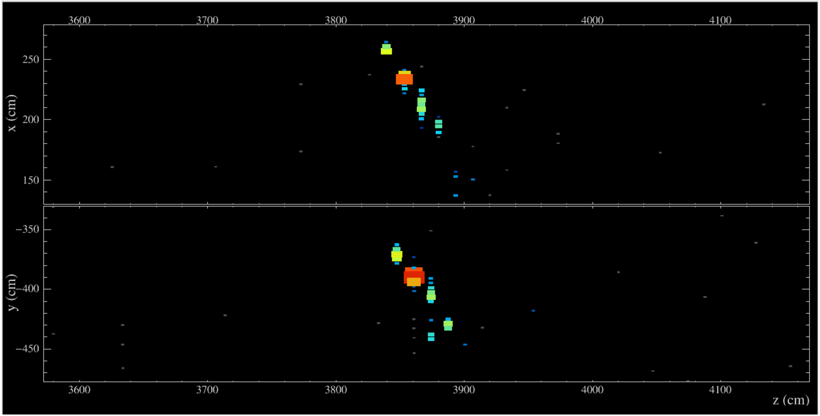

Some Selected Candidates

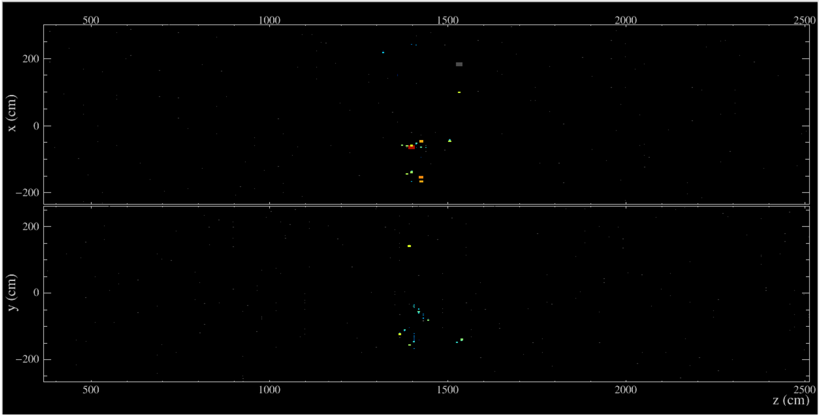

Data-Driven Background Estimation

Use visible energy side-band to constrain the background normalization.

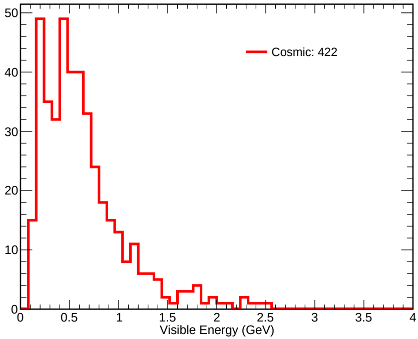

Figure 13: Distribution of visible energy from the FD real data after all but the visible energy cut are applied. Side-band regions used for the estimation of the background will be defined based on this distribution.

Data-Driven Background Estimation

- We only look at the region 0.5-2 GeV. The signal region is 0.9-1.6 GeV. The side-band is 0.5-0.9 GeV and 1.6-2 GeV.
- Fit side-band with an exponential function of the visible energy, see next slide.
- The total number of events in the side-band region is counted as B_{sb}. By a simple algebra, we can find the B_{sig} of the background in the signal region as

$$B_{\text{sig}} = B_{\text{sb}} \times \frac{1-x}{x}, \tag{8}$$

in which, x is the normalized area under the curve of the fit function in the side-band region.

Data-Driven Background Estimation

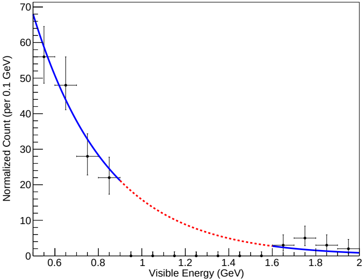

Figure 14: The side-band region is fitted with an exponential function. There are $B_{\text{sb}} = 167$ events in the side-band. Area under the fitting curve in side-band region is $x = 0.73$.

- From (8), we find $B_{\text{sig}} = 63.21$ events.
- We observed 63 events in the signal region. Agreement with "all-background" assumption.

Sensitivity Calculation

	λ (n.yrs)	ϵ	b
Mean Value	2.1×10^{34}	11.5%	1330
Assumed Error (Percentage)	1%	10%	30%
Assumed Error	2.1×10^{32}	1.2%	400

Table 5: Figures needed for NOvA's sensitivity calculation assuming 10 years of exposure.

Furthermore, we assumed a nuclear suppression factor $R = 0.53 \times 10^{23}$ s^{-1} for ^{12}C nucleus.

- Null result is assumed with the number of observed events is equal to the number of estimated background.
- Systematic errors have not been analyzed. Conservative guesses are made.

Sensitivity Calculation

Using Bayesian approach, the posterior of the true event rate is

$$
\begin{aligned}
P(\Gamma|n) = A \int_0^{+\infty} \int_0^1 \int_{-\infty}^{+\infty} & \frac{(\Gamma\lambda\epsilon + b)^n}{n!} \\
& \times \exp\left[-(\Gamma\lambda\epsilon + b) - \frac{(\lambda-\lambda_0)^2}{2\sigma_\lambda^2} - \frac{(\epsilon-\epsilon_0)^2}{2\sigma_\epsilon^2} - \frac{(b-b_0)^2}{2\sigma_b^2} \right] \\
& \times \; \mathrm{d}b \, \mathrm{d}\epsilon \, \mathrm{d}\lambda.
\end{aligned}
$$

The 90% confidence limit of the event rate $\Gamma_{90\%}$ can be found by solving for

$$\int_0^{\Gamma_{90\%}} P(\Gamma|n) \, \mathrm{d}\Gamma = 0.9. \tag{9}$$

Numerical integration is performed by the multi-dimensional integration toolkit `Cubature`.

Results

1. 90% C.L. limit on event rate

$$\Gamma_{90\%} = 2.455 \times 10^{-31} \ (\mathrm{year}^{-1}).$$

2. 90% C.L. limit on oscillation time of bound neutrons in ^{12}C

$$T_{90\%} = \frac{1}{\Gamma_{90\%}} = 4 \times 10^{30} \ (\mathrm{year}).$$

3. 90% C.L. limit on oscillation time of free neutrons

$$\tau_{90\%} = \sqrt{\frac{T_{90\%}}{R}} = 0.57 \times 10^{8} \ (s).$$

Conclusions

Experiment	Source of neutrons	T (yr)	τ (s)
ILL	neutron beam		0.9×10^8
Soudan	^{56}Fe	0.72×10^{32}	1.3×10^8
Frejus	^{56}Fe	0.65×10^{32}	1.2×10^8
Kamiokande	^{16}O	0.43×10^{32}	1.2×10^8
Super-K	^{16}O	1.90×10^{32}	2.7×10^8
SNO	^{2}D	1.48×10^{31}	1.4×10^8
NOvA	^{12}C	4.07×10^{30}	0.6×10^8

Table 6: Experimental limits on neutron oscillation life-time.

This limit shows that, to the first order, we are going in the right direction. However, comparing the current NOvA's result to past experiment, it is clear that many aspects of the analysis need to be improved if we want to achieve a higher competitiveness.

Future Work

Neutron-Antineutron Oscillation Analysis

- Complete the background modelling based on simulation of atmospheric neutrinos and cosmogenic neutrons.
- Identify and evaluate the effects of systematic uncertainties.
- Improve the event reconstruction with prong reconstruction and possibly prong ID.
- Improve the event selection using multivariate methods.

Backup slides

Neutron Oscillation Probability Calculations

The time-evolution matrix $\mathrm{e}^{-\mathrm{i}At}$ can be computed via its series expansion

$$\mathrm{e}^{-\mathrm{i}At} = 1 + \frac{-\mathrm{i}At}{1!} + \frac{(-\mathrm{i}At)^2}{2!} + \frac{(-\mathrm{i}At)^3}{3!} + \cdots$$

To compute the exact expression, A can be written as

$$A = \begin{pmatrix} E_n & \delta m \\ \delta m & E_n \end{pmatrix} = \frac{1}{2}(2\delta m \cdot \sigma_x + \Delta E \cdot \sigma_z) + \frac{1}{2}(E_n + E_{\bar{n}}) \cdot I,$$

where σ_x and σ_z are Pauli matrices

$$\sigma_x = \begin{pmatrix} 0 & 1 \\ 1 & 0 \end{pmatrix}, \sigma_z = \begin{pmatrix} 1 & 0 \\ 0 & -1 \end{pmatrix}$$

which satisfy $\sigma_x^2 = \sigma_x^2 = I$, and $\Delta E = E_n - E_{\bar{n}}$.

Neutron Oscillation Probability Calculations

Thanks to this decomposition, now we have

$$e^{-\mathrm{i}At} = e^{-\frac{\mathrm{i}t}{2}(E_n+E_{\bar{n}})\cdot I} \cdot e^{-\frac{\mathrm{i}t}{2}(2\delta m\cdot\sigma_x+\Delta E\cdot\sigma_z)}.$$

The first factor only provides a phase shift

$$e^{-\frac{\mathrm{i}t}{2}(E_n+E_{\bar{n}})\cdot I} = e^{-\frac{\mathrm{i}t}{2}(E_n+E_{\bar{n}})} \cdot I,$$

which would disappear when the absolute value is taken.

Neutron Oscillation Probability Calculations

To expand the second term, we need to rely on the following property of the Pauli's matrices

$$(a \cdot \sigma_x + b \cdot \sigma_z)^n = \begin{cases} \gamma^n \cdot I & \text{for even } n, \\ \gamma^n \cdot \left(\dfrac{a \cdot \sigma_x + b \cdot \sigma_z}{\gamma} \right) & \text{for odd } n, \end{cases}$$

in which $\gamma = \sqrt{a^2 + b^2}$.

Neutron Oscillation Probability Calculations

Apply these identities to our case with $a = 2\delta m$ and $b = \Delta E$, the expansion can then be reduced to

$$
\begin{aligned}
& e^{-\frac{\mathrm{i}t}{2}(2\delta m\cdot\sigma_x+\Delta E\cdot\sigma_z)} = \\
& I\cdot\left[1-\frac{(\gamma t/2)^2}{2!}+\frac{(\gamma t/2)^4}{4!}-\cdots\right] \\
& -\mathrm{i}\left(\frac{2\delta m\cdot\sigma_x+\Delta E\cdot\sigma_z}{\gamma}\right)\cdot\left[\frac{(\gamma t/2)}{1!}-\frac{(\gamma t/2)^3}{3!}+\cdots\right] \\
& = \cos\frac{\gamma t}{2}\cdot I - i\sin\frac{\gamma t}{2}\cdot\left(\frac{2\delta m\cdot\sigma_x+\Delta E\cdot\sigma_z}{\gamma}\right).
\end{aligned}
$$

Neutron Oscillation Probability Calculations

The probability of a neutron oscillating to an antineutron given by

$$
\begin{aligned}
P_{\bar{n}}(t) &= \left| < \bar{n} | e^{-\mathrm{i}At} | n > \right|^2 \\
&= \left| \begin{pmatrix} 0 & 1 \end{pmatrix} \begin{pmatrix} \cos\left(\frac{\gamma t}{2}\right) - i\frac{\Delta E}{\gamma}\sin\left(\frac{\gamma t}{2}\right) & -i\frac{2\delta m}{\gamma}\sin\Big(\\ -i\frac{2\delta m}{\gamma}\sin\left(\frac{\gamma t}{2}\right) & \cos\left(\frac{\gamma t}{2}\right) + i\frac{\Delta E}{\gamma} \end{pmatrix} \right. \\
&= \frac{4\delta m^2}{\gamma^2}\sin^2\left(\frac{\gamma t}{2}\right) \\
&= \frac{4\delta m^2}{4\delta m^2 + \Delta E^2}\sin^2\left(\frac{\sqrt{4\delta m^2 + \Delta E^2}}{2}t\right) .
\end{aligned}
$$

Neutron Oscillation Probability Calculations

With the oscillation of free neutrons $t\sqrt{\Delta E^2 + \delta m^2} \ll 1$, the oscillation probability becomes

$$P_{\bar{n}}(t) \sim \frac{4\delta m^2}{\Delta E^2 + 4\delta m^2} \left(\frac{\sqrt{\Delta E^2 + 4\delta m^2}}{2} t \right)^2$$
$$= (\delta m \cdot t)^2 \equiv \left(\frac{t}{\tau_{n\bar{n}}} \right)^2 ,$$

Neutrino Physics at NOvA

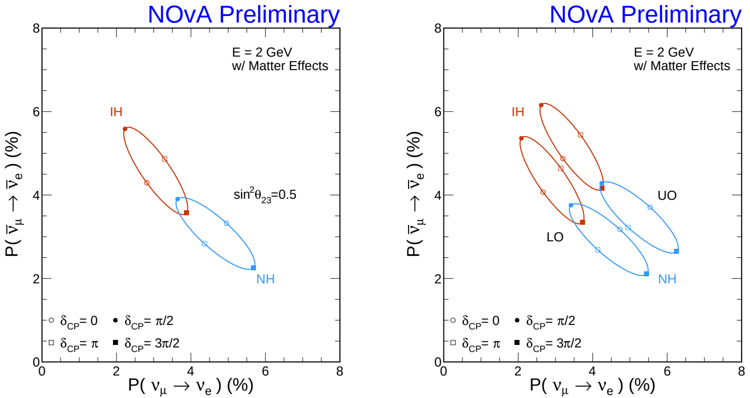

Figure 15: Bi-probability plots of ν_e and $\bar{\nu}_e$ appearances in NOvA.

Data-Driven Trigger System in NOvA

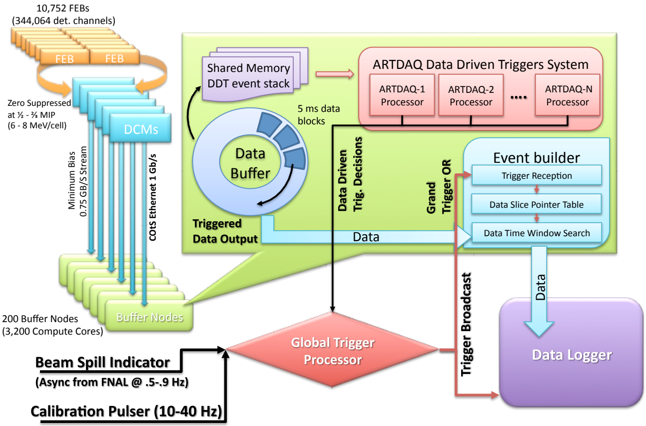

Figure 16: A schematic overview of the FD DAQ system.

Trigger Selection Cuts

Hit Extent Asymmetry

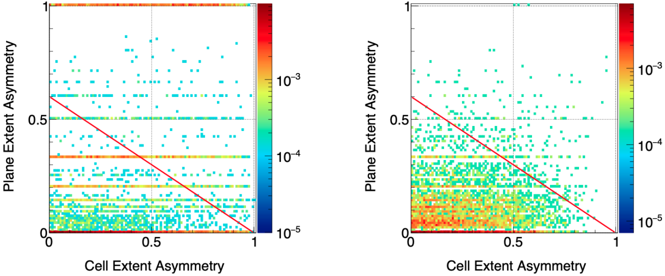

(a) cosmic (b) signal

Figure 17: Events above the red curve are cut off (28% of cosmic rays and 5% of signal candidates). This selection cut mainly targets the cosmic rays which extends the whole length of the detector ($a_Z = 1$) or over many planes.

Proton Decay Energy Probe

Typical proton decay has an operator of the form $gqqql/\Lambda^2$. g is a dimensionless coupling constant. Λ is the UV-cutoff the energy scale probed. The rate of this decay is $\Gamma \propto (m_p^\alpha/\Lambda^2)^2$ and must have a dimension of energy so $\alpha = 5/2$. The current limit on proton life time of 10^{34} means the energy probed is at the GUT scale:

$$\Lambda \propto \sqrt[4]{\frac{m_p^5}{\Gamma}} \approx \sqrt[4]{\frac{1\ \text{GeV}^5}{(10^{34}\cdot 31.5\times 10^6\cdot 1.52\times 10^{24})^{-1}\ \text{GeV}}}$$
$$= 2.6\times 10^{16}\ \text{GeV}.$$

SI to Natural: $1\,\text{GeV} \approx 1.52\times 10^{24}\ \text{s}^{-1}$ and $1\,\text{year} \approx 31.5\times 10^6\ \text{s}$.

Proton Decay Energy Probe

Typical proton decay has an operator of the form $gqqql/\Lambda^2$. g is a dimensionless coupling constant. Λ is the UV-cutoff the energy scale probed. The rate of this decay is $\Gamma \propto (m_p^\alpha/\Lambda^2)^2$ and must have a dimension of energy so $\alpha = 5/2$. The current limit on proton life time of 10^{34} means the energy probed is at the GUT scale:

$$\Lambda \propto \sqrt[4]{\frac{m_p^5}{\Gamma}} \approx \sqrt[4]{\frac{1 \text{ GeV}^5}{(10^{34} \cdot 31.5 \times 10^6 \cdot 1.52 \times 10^{24})^{-1} \text{ GeV}}}$$
$$= 2.6 \times 10^{16} \text{ GeV}.$$

SI to Natural: $1\,\text{GeV} \approx 1.52 \times 10^{24}\ \text{s}^{-1}$ and $1\,\text{year} \approx 31.5 \times 10^6$ s.

Neutron Oscillation Energy Probe

A neutron-antineutron transition features an operator of the form $gqqq\bar{q}\bar{q}\bar{q}/\Lambda^5$. Using similar dimensional analysis, the transition rate is $\Gamma \propto m_n^{11}/\Lambda^{10}$. The current limits on the oscillation time of free neutrons around 10^8 s implies a UV-cutoff

$$\Lambda \propto \sqrt[10]{\frac{m_n^{11}}{\Gamma}} \approx \sqrt[10]{\frac{1 \text{ GeV}^{11}}{(10^8 \cdot 1.52 \times 10^{24})^{-1} \text{ GeV}}} = 1.6 \times 10^3 \text{ GeV},$$

SI to Natural: $1\,\text{GeV} \approx 1.52 \times 10^{24}\ \text{s}^{-1}$ and $1\,\text{year} \approx 31.5 \times 10^6$ s.

Sensitivity Calculation

Bayesian Method

This analysis is an counting experiment. The expected number of candidates will be given by

$$\mu = \Gamma \lambda \epsilon + b, \tag{10}$$

where Γ is the true event rate, λ is the true exposure, ϵ is the true signal efficiency and b is the true mean of background estimation.

The probability of observing n candidate events follows a Poisson distribution with the mean of μ:

$$P(n|\mu) = \frac{e^{-\mu}\mu^n}{n!} = \frac{e^{-(\Gamma\lambda\epsilon+b)}(\Gamma\lambda\epsilon+b)^n}{n!}. \tag{11}$$

Sensitivity Calculation

Bayesian Method

Bayes theorem leads to

$$P(\mu(\Gamma, \lambda, \epsilon, b)|n) \cdot P(n) = P(n|\mu(\Gamma, \lambda, \epsilon, b)) \cdot P(\mu(\Gamma, \lambda, \epsilon, b)).$$

Because $\Gamma, \lambda, \epsilon, b$ are independent

$$P(\mu(\Gamma, \lambda, \epsilon, b)) = P(\Gamma) \cdot P(\lambda) \cdot P(\epsilon) \cdot P(b).$$

We can calculate the posterior of the true event rate by integral

$$\begin{aligned} P(\Gamma|n) &= \int P(\mu(\Gamma, \lambda, \epsilon, b)|n) \, \mathrm{d}\lambda \, \mathrm{d}\epsilon \, \mathrm{d}b, \qquad (12) \\ &= A \int P(n|\mu(\Gamma, \lambda, \epsilon, b)) \cdot P(\mu(\Gamma, \lambda, \epsilon, b)) \, \mathrm{d}\lambda \, \mathrm{d}\epsilon \, \mathrm{d}b, \\ &= A \int \frac{e^{-(\Gamma\lambda\epsilon + b)}(\Gamma\lambda\epsilon + b)^n}{n!} P(\Gamma) \; P(\lambda) \; P(\epsilon) \; P(b) \, \mathrm{d}\lambda \, \mathrm{d}\epsilon \, \mathrm{d}b. \end{aligned}$$

Sensitivity Calculation
Bayesian Method

The normalization factor A can be determined by constraint the posterior probability

$$\int_0^{\infty} P(\Gamma|n)\,\mathrm{d}\Gamma = 1. \tag{13}$$

The 90% confidence limit of the event rate $\Gamma_{90\%}$ can be found by solving for

$$\int_0^{\Gamma_{90\%}} P(\Gamma|n)\,\mathrm{d}\Gamma = 0.9. \tag{14}$$

Once the limit of the event rate is found, the limit of the oscillation lifetime is simply the inversion of the rate.

Sensitivity Calculation

Bayesian Priors

The priors $P(\Gamma), P(\lambda), P(\epsilon), P(b)$ are used to include the systematic effects into the calculation of the limit. In this sensitivity study, we took them as Gaussians, truncated in the unphysical regions of the corresponding parameters.

$$P(\lambda) \propto \exp\left[-\frac{(\lambda-\lambda_0)^2}{2\sigma_\lambda^2}\right] \tag{15}$$

$$P(\epsilon) \propto \exp\left[-\frac{(\epsilon-\epsilon_0)^2}{2\sigma_\epsilon^2}\right] \tag{16}$$

$$P(b) \propto \exp\left[-\frac{(b-b_0)^2}{2\sigma_b^2}\right]. \tag{17}$$

Values of λ_0, ϵ_0, b_0, σ_λ, σ_ϵ and σ_b come from Table 5.

Selection Variables

Hit Counts in XZ view

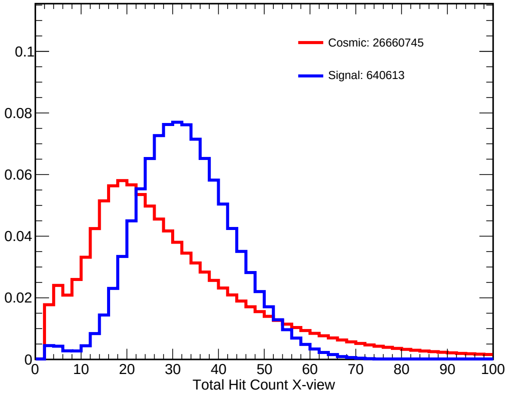

Figure 18: Hit counts in XZ view of the simulated events (blue) and the FD data's signal-like events (red).

Selection Variables

Hit Counts in *YZ* view

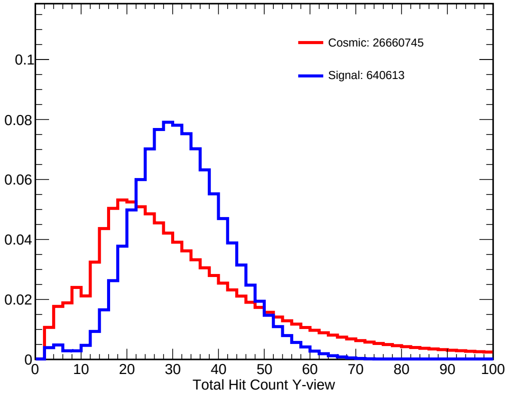

Figure 19: Hit counts in *YZ* view of the simulated events (blue) and the FD data's signal-like events (red).

Selection Variables

Hit Count Difference Between Views

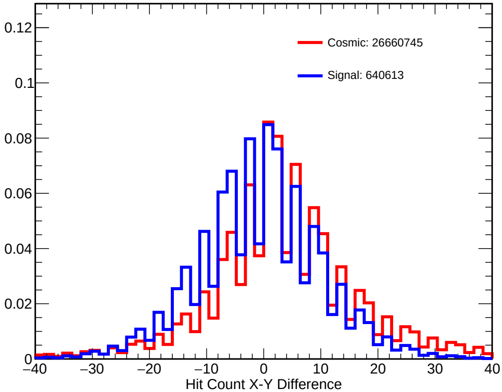

Figure 20: Hit count difference ($N_{YZ} - N_{XZ}$) of the simulated events (blue) and the FD data's signal-like events (red).

Selection Variables

Visible Energy

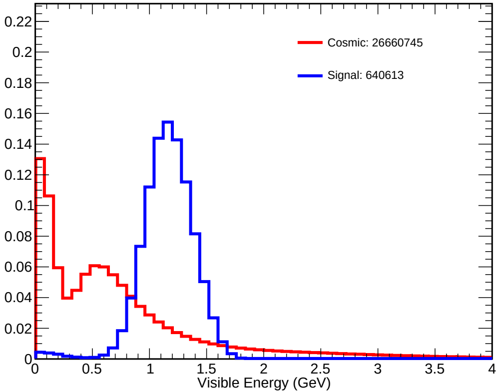

Figure 21: Visible energy (in GeV) distributions of the simulated events (blue) and the FD data's signal-like events (red).

Selection Variables

Average Hit Energy in *XZ* view

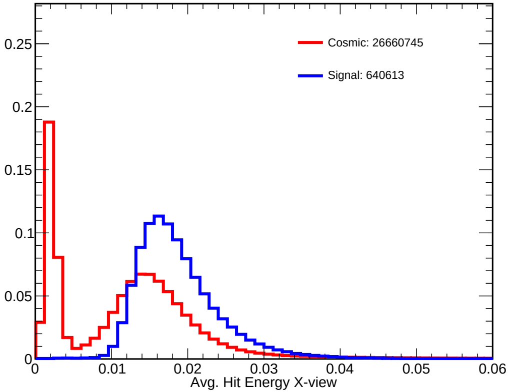

Figure 22: Distributions of average hit energy (in GeV) in *XZ* of the simulated events (blue) and the FD data's signal-like events (red).

Selection Variables

Average Hit Energy in *YZ* view

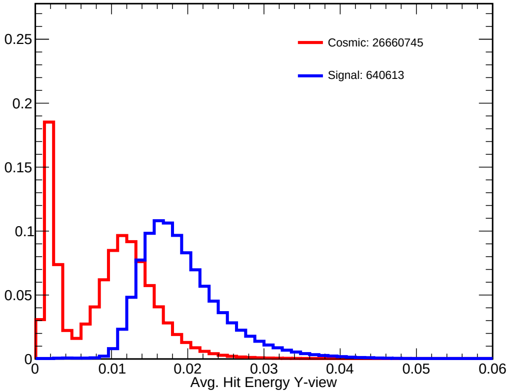

Figure 23: Distributions of average hit energy (in GeV) in *YZ* of the simulated events (blue) and the FD data's signal-like events (red).

Selection Variables

Event Duration

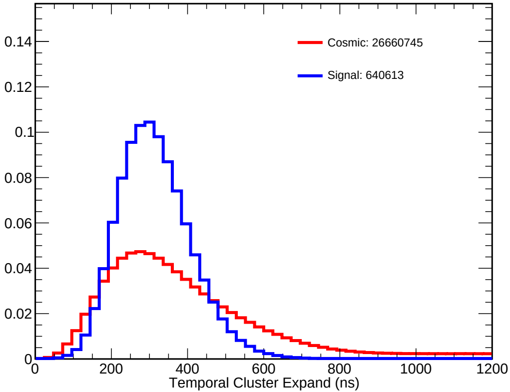

Figure 24: Time duration (in ns) distributions of the simulated events (blue) and the FD data's signal-like events (red).

Selection Variables

Cell Hit Position-Timing Correlation

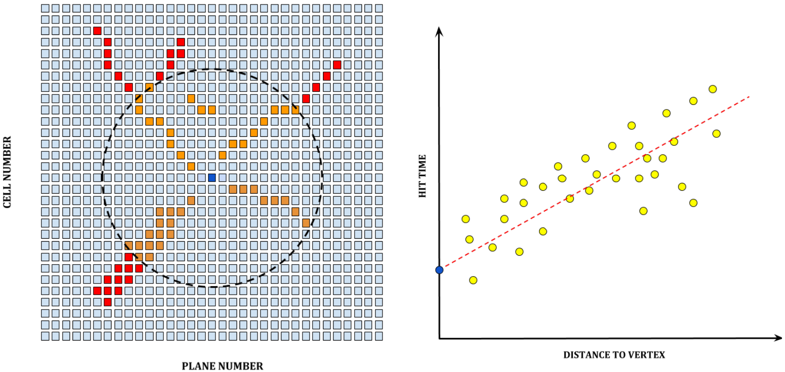

Figure 25: Dashed circle centers the vertex and sum up 90% of total energy. Hits within this region is used to calculate the position-timing correlation.

Selection Variables

Cell Hit Position-Timing Correlation

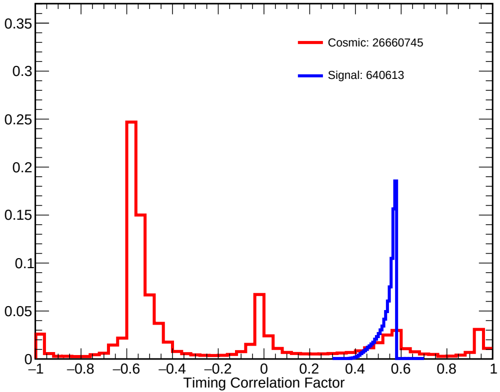

Figure 26: Hit position-timing correlation distributions of the simulated events (blue) and the FD data's signal-like events (red).

Selection Variables

Vertex y

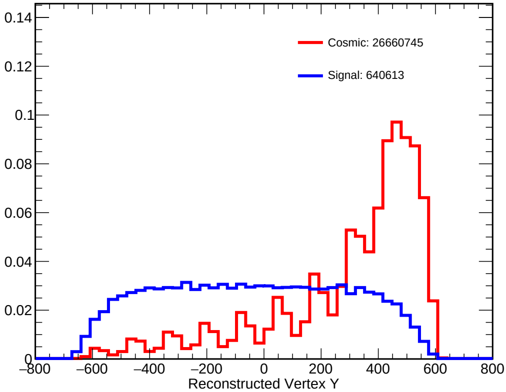

Figure 27: Vertex y position (in cm) distributions of the simulated events (blue) and the FD data's signal-like events (red).

Selection Variables

Hit Counts in *XZ* view

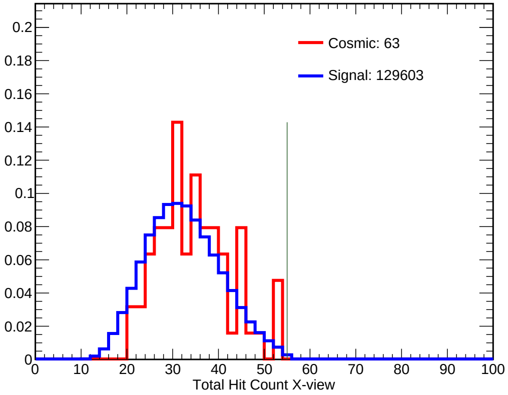

Figure 28: Hit counts in *XZ* view of the simulated events (blue) and the FD data's signal-like events (red) after selection cuts.

Selection Variables

Hit Counts in *YZ* view

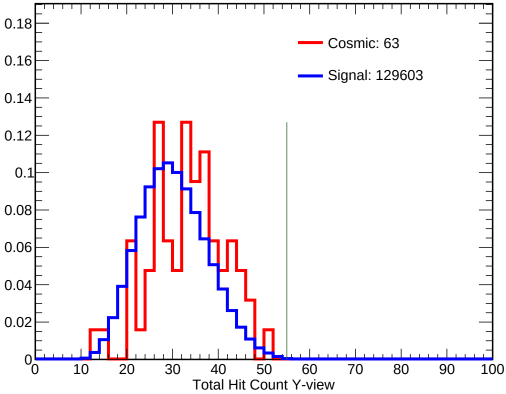

Figure 29: Hit counts in *YZ* view of the simulated events (blue) and the FD data's signal-like events (red) after selection cuts.

Selection Variables

Hit Count Difference Between Views

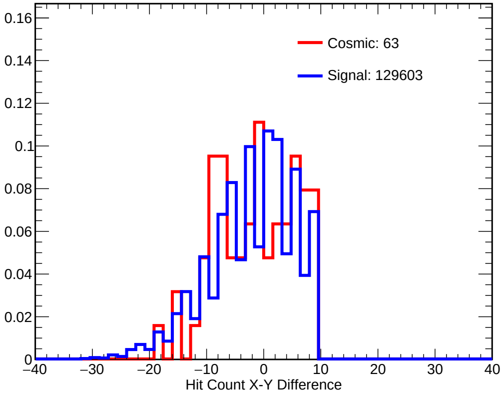

Figure 30: Hit count difference $(N_{YZ} - N_{XZ})$ of the simulated events (blue) and the FD data's signal-like events (red) after selection cuts.

Selection Variables

Visible Energy

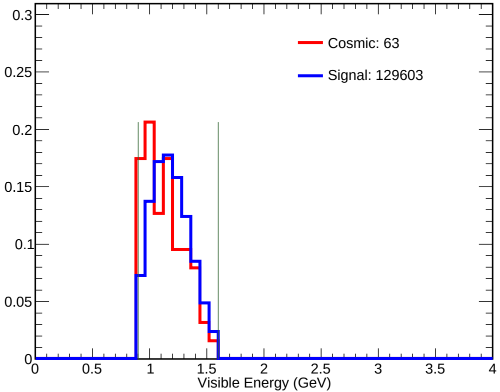

Figure 31: Visible energy (in GeV) distributions of the simulated events (blue) and the FD data's signal-like events (red) after selection cuts.

Selection Variables

Average Hit Energy in *XZ* view

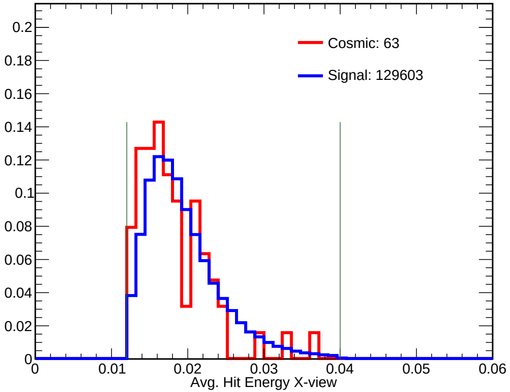

Figure 32: Average hit energy (in GeV) in *XZ* of the simulated events (blue) and the FD data's signal-like events (red) after selection cuts.

Selection Variables

Average Hit Energy in *YZ* view

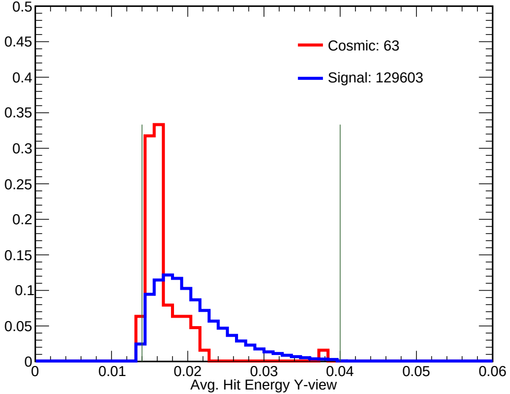

Figure 33: Average hit energy (in GeV) in *YZ* of the simulated events (blue) and the FD data's signal-like events (red) after selection cuts.

Selection Variables

Event Duration

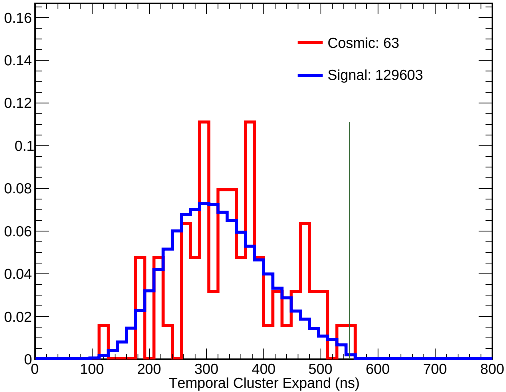

Figure 34: Time duration (in ns) of the simulated events (blue) and the FD data's signal-like events (red) after selection cuts.

Selection Variables

Cell Hit Position-Timing Correlation

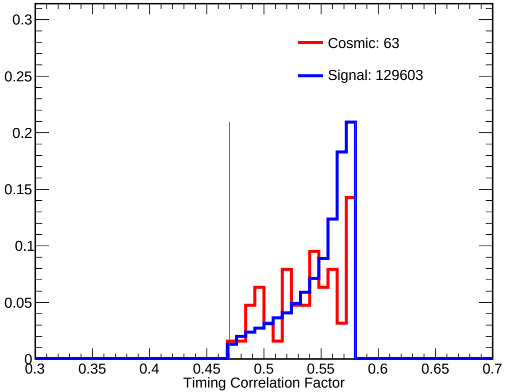

Figure 35: Hit position-timing correlation of the simulated events (blue) and the FD data's signal-like events (red) after selection cuts.

Selection Variables

Vertex y

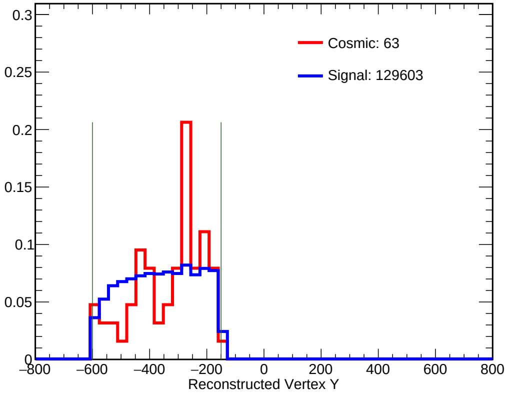

Figure 36: Vertex y position (in cm) of the simulated events (blue) and the FD data's signal-like events (red) after selection cuts.

TDU Online Timing Calibration

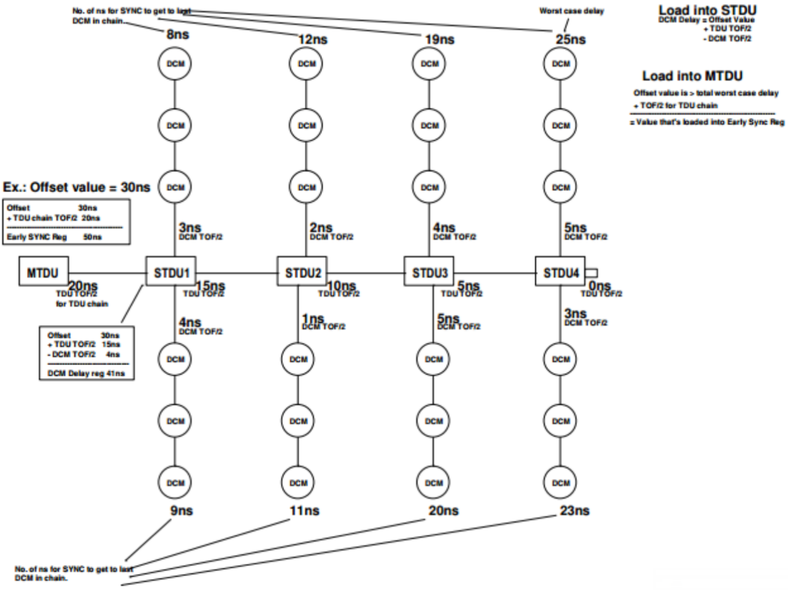

Offline Timing Calibration Crosscheck

- Use cosmic muon tracks that pass through multiple DCMs (and other 8 quality selection cuts).
- The relative time differences (offsets) between hits in different DCMs is calculated.
- A matrix of these relative differences in inverted to solve for the absolute timing offsets between each DCM in the detector and a fixed reference DCM.
- If the synchronization described previously is performed properly all the absolute offsets should come out to zero.

Details: see here

Timing Calibration

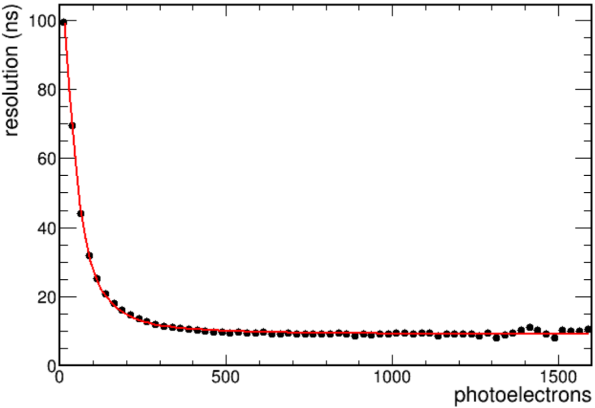

Figure 37: Timing resolution determined from Far Detector data.

Timing Calibration

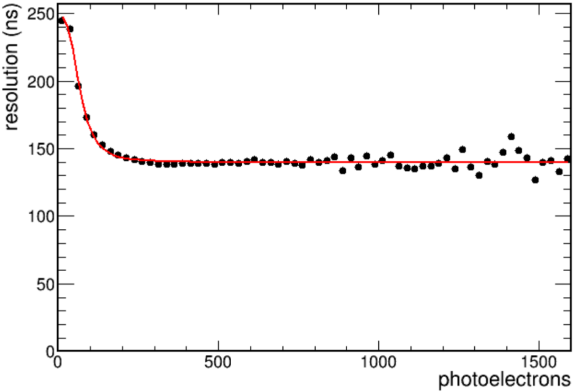

Figure 38: Timing resolution determined from Far Detector data (using simple DCS sampling).

Timing Calibration

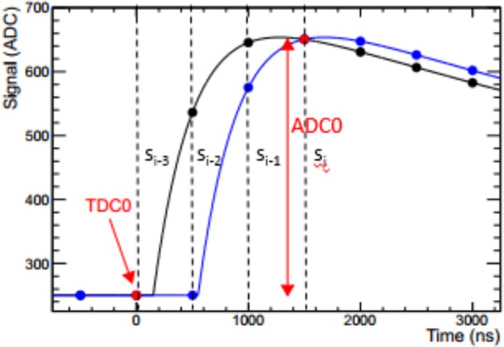

Figure 39: The ASIC on each FEB shapes the pulse signal from the APD with a 460 ns rise-time and 7000 ns fall-time at the FD where the signal is sampled every 500 ns.

True Vertex Position-Timing Correlation